AMERICAN SOCIETY FOR MICROBIOLOGY | Applied and Environmental Microbiology®

MICROBIAL ECOLOGY

In Vivo Single-Cell Fluorescence and Size Scaling of Phytoplankton Chlorophyll Content

Eva Álvarez,* Enrique Nogueira, Ángel López-Urrutia

Instituto Español de Oceanografía, Centro Oceanográfico de Gijón, Gijón, Asturias, Spain

ABSTRACT In unicellular phytoplankton, the size scaling exponent of chlorophyll content per cell decreases with increasing light limitation. Empirical studies have explored this allometry by combining data from several species, using average values of pigment content and cell size for each species. The resulting allometry thus includes phylogenetic and size scaling effects. The possibility of measuring single-cell fluorescence with imaging-in-flow cytometry devices allows the study of the size scaling of chlorophyll content at both the inter- and intraspecific levels. In this work, the changing allometry of chlorophyll content was estimated for the first time for single phytoplankton populations by using data from a series of incubations with monocultures exposed to different light levels. Interspecifically, our experiments confirm previous modeling and experimental results of increasing size scaling exponents with increasing irradiance. A similar pattern was observed intraspecifically but with a larger variability in size scaling exponents. Our results show that size-based processes and geometrical approaches explain variations in chlorophyll content. We also show that the single-cell fluorescence measurements provided by imaging-in-flow devices can be applied to field samples to understand the changes in the size dependence of chlorophyll content in response to environmental variables affecting primary production.

IMPORTANCE The chlorophyll concentrations in phytoplankton register physiological adjustments in cellular pigmentation arising mainly from changes in light conditions. The extent of these adjustments is constrained by the size of the phytoplankton cells, even within single populations. Hence, variations in community chlorophyll derived from photoacclimation are also dependent on the phytoplankton size distribution.

KEYWORDS FlowCam, chlorophyll, fluorescence, irradiance, photosynthetic pigments, primary production, single cell, size scaling

Received 7 December 2016 **Accepted** 12 January 2017

Accepted manuscript posted online 23 January 2017

Citation Álvarez E, Nogueira E, López-Urrutia Á. 2017. *In vivo* single-cell fluorescence and size scaling of phytoplankton chlorophyll content. Appl Environ Microbiol 83:e03317-16. https://doi.org/10.1128/AEM.03317-16.

Editor Robert M. Kelly, North Carolina State University

Address correspondence to Eva Álvarez, eva.alvarez.suarez@gmail.com.

* Present address: Eva Álvarez, Alfred-Wegener-Institut, Helmholtz-Zentrum für Polar- und Meeresforschung, Bremerhaven, Germany.

The growth rate of phytoplankton cells in the oceans is limited by the availability of resources, such as light and nutrients (1). In order to maximize the efficiency of resource acquisition in a variable environment, cell physiology adjusts through a suite of acclimation processes. Photoacclimation refers to the phenotypic adjustments of the cells in response to variations in irradiance levels, and it is typically reflected in a graded reduction in the photosynthetic pigment content with increasing irradiance (2). The mechanistic basis for the pigment content-irradiance relationship is well known (3, 4) and leads to altered cellular pigment composition.

Because all phototrophic plankton contain chlorophyll *a* (Chl *a*) as a light-harvesting pigment, it is arguably the best known and most widely used proxy for autotrophic biomass (5). However, changes in the ratio of Chl *a* to carbon biomass indicate an adjustment of cellular pigment levels to match the demands for photosynthesis (6), and the concentration of Chl *a* is thus a biased estimator of phytoplankton biomass

expressed in organic carbon terms (1). Instead, the intracellular Chl *a* concentration can give a vision of the physiological status of the cells that can be translated to the community level.

Phytoplankton cells adjust the Chl *a*-to-carbon biomass ratio (Chl *a*/C ratio) in response to an imbalance between the rate of light absorption and the energy demands for photosynthesis and biosynthesis (7). Hence, the Chl *a*/C ratio varies in response to changes not only in light but also in growth rate (6). A reduction in growth rate increases the Chl *a*/C ratio, and growth rate explained 39% of the variability in the Chl *a*/C ratio (8). Nutrient availability also influences the Chl *a*/C ratio (9), since chlorophyll synthesis is a function of the nitrogen status (10). Regarding taxonomy, the average Chl *a*/C ratio differs for different taxonomical groups of phytoplankton (11).

Light utilization traits, such as pigment content, are thought to be explained in part by cell size (12, 13). When resources are limiting, the cell surface area-to-volume ratio imposes fundamental constraints on the rates of resource acquisition (14). The "package" effect is defined as a reduction in the absorption of pigmented particles within a cell relative to the absorption of the same pigments in solution. The explanation is purely geometrical: as cell volume increases, internal optical path lengths increase, limiting the absorptive efficiency of Chl *a* molecules through self-shading, and, as a result, larger cells tend to have relatively lower intracellular concentrations of Chl *a* than smaller cells to limit shading effects due to the packaging of pigments (13, 15). This translates into a size dependence of Chl *a* content that has been reported in laboratory experiments (16) and field studies (17, 18). Additionally, cell size can vary with irradiance and the phase of cellular cycle (19), and hence, changes in pigment content can be due to changes in size and not just to photoacclimation processes. It is, then, crucial to consider the cellular size when dealing with changes in the elemental composition of phytoplankton.

The size dependence of the photoacclimation response results in different allometric exponents in the size scaling of Chl *a* content with changing irradiance (15). The photosynthetic response to varying irradiance has been described theoretically as a function of cell size (V), considering an optimal light-harvesting strategy (15) and calculating the intracellular pigment concentration required to maximize photosynthesis for a given cell size and a given irradiance. The model predicted that the optimal chlorophyll concentration is proportional to $V^{3/4}$ under light saturation and to $V^{2/3}$ under light limitation. The prediction of different allometric exponents was tested using data from different species cultured in the laboratory (20), which does not permit exclusion of the variability due to taxonomical composition. The calculation of allometric exponents on a single-cell basis allows testing of this prediction in single populations. Hence, evaluation of the same species along its whole size range allows one to observe the size dependence of chlorophyll content without the effect of interspecific variability.

The cell-level perspective provided by flow cytometry and the capacity to measure large numbers of cells has been used extensively by biological oceanographers to define the distributions and dynamics of marine picophytoplankton. Flow cytometry techniques have allowed the quantification of optical properties, such as Chl *a* autofluorescence, on individual cells (21). Chl *a* absorbs energy from light and releases it through several phenomena, one of them being the emission of fluorescence in the red portion of the spectrum; thus, the fluorescence of Chl *a* reflects the endogenous concentration of this pigment. This is the rationale for the estimation of Chl *a in situ* by means of fluorometers (22) or for the measurement of discrete samples by means of fluorometric methods (23). Chl *a* fluorescence intensity quantified by flow cytometry has been shown to scale with cellular Chl *a* levels in nanophytoplankton (24), but the relationships reported are not constant for all taxa due to differences in intracellular pigment structure or, even for the same taxon, due to differences in growth conditions. Hence, none of these studies provide a taxon-independent conversion from fluorescence to Chl *a* that can be applied to natural samples.

In addition, traditional flow cytometers have a limited capacity to analyze large phytoplankton (>5 μm). There are no measurements of single-cell fluorescence for microplankton, a size range in which a significant proportion of the autotrophic activity takes place. The flow cytometer and microscope instrument (FlowCam) provides an automated technique for plankton enumeration that combines flow cytometry and microscopy (25). Although the FlowCam is not a flow cytometer *per se*, it contains the needed elements to measure the fluorescent response of single cells: a source of light, a fluidics system in which the cells are embedded, and a detection sensor. When a suspension of phototrophic cells runs through the fluidics system, the detected fluorescence signals trigger the digital camera to obtain images that allows counting and sizing of the cells in the sample. However, the fluorescence signals measured by the FlowCam have not yet been interpreted beyond determination of cell viability (26).

Here, we present a reliable methodology for the estimation of the content of Chl *a* on single cells that allows the exploration of the changes in size scaling of Chl *a* content when cells are exposed to light limitation and that can be applied to field studies. Seven species of marine phytoplankton were grown over a range of irradiances and nonlimiting nutrient conditions, and their content in pigments and fluorescence was monitored to describe the relationship between the FlowCam-measured fluorescence per cell and the content of Chl *a* per cell. With those cultured species, we explored the changes in the interspecific and intraspecific size scaling of Chl *a* content. Finally, the size scaling of Chl *a* content in field samples was explored and related to the irradiance levels in the water column. Our results show that the allometry of the content of Chl *a* changed with light intensity. This physiological response and the size dependence of Chl *a* content can be monitored in field samples due to the measurement of Chl *a* content on a single-cell basis with imaging-in-flow devices.

RESULTS

Variability of the fluorescence signal. Experiments 1 to 4 each took place in two parallel incubator lines, thereby allowing the treatments to be analyzed in duplicate (line replicate). Additionally, in experiment 1, samples of the first line were analyzed in duplicate (aliquot replicate). These results were used to account for the variability in the fluorescence signal detected by the FlowCam. Fluorescent beads analyzed each sampling day (between 64 and 768 items) presented average values of 181 $\pm$ 14 fluorescence units with the 20$\times$ lens and of 41 $\pm$ 19 fluorescence units with the 10$\times$ lens. The variability between average values in parallel incubations (Fig. 1A) was $\pm$38 fluorescence units per cell (95% confidence interval [CI]), whereas the variability between aliquots in the same incubation line (Fig. 1B) was $\pm$4 fluorescence units per cell. The standard deviation within each FlowCam run was in all cases higher than the differences in average values between experimental (line or aliquot) replicates. This indicates that the fluorescence signal was constant enough to compare different experiments or treatments (interspecific variation) and sensitive enough to distinguish differences among cells of the same population (intraspecific variation).

Phytoplankton incubations. Experiments 5 to 12 were used to obtain a fluorescence-to-Chl *a* conversion and to explore the inter- and intraspecific scaling of chlorophyll content. Although the number of generations experienced in each experiment from the beginning to the last day was variable (Table 1), the experiments that also sampled twice in the midterm (days 8 and 11) confirmed that the relative composition of the cells was constant for most of the light treatments from the midterm sample to the sample at the end of the incubation, indicating that the cells were already acclimated to culture conditions (Fig. 2).

The average fluorescence per unit volume and the average intracellular Chl *a* concentration on the last day of incubation varied as a function of growth irradiance (Fig. 3) in all experiments. The pigment concentration obtained through Chl *a* extraction decreased as expected with increased irradiance, and the same pattern was captured by the FlowCam-measured fluorescence: fluorescence intensity decreased with irradiance in parallel with intracellular pigment content. The only exception was

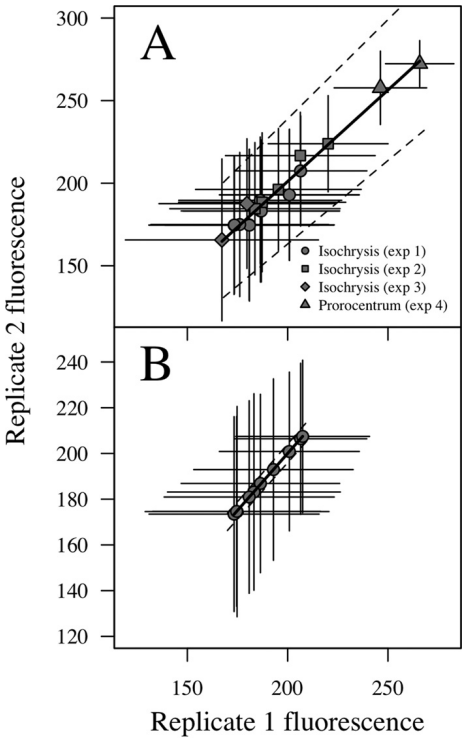

FIG 1 Variability (mean ± SD) of the fluorescence signal within parallel lines of the incubator during experiments 1 to 4 (A) and duplicate sample analysis during experiment 1 (B). Dashed lines indicate the 95% confidence interval.

experiment 11, which showed higher fluorescence at intermediate growth irradiances but which maintained the general decreasing pattern for higher values.

Fluorescence-to-Chl *a* conversion. To explore the relationship between the fluorescence measured by the FlowCam and the Chl *a* content, we analyzed the relationship between the average (peak) fluorescence per cell (arbitrary units cell^{-1}) and the average intracellular pigment content per cell (picograms of Chl *a* cell^{-1}) on the last day of the incubation experiments (Fig. 4). Since the fluorescence signals measured with different combinations of FlowCam magnification lenses and flow chamber dimensions (FC) were not comparable due to optical differences, the relationship was explored for each of the applied combinations (200×/FC50 and 100×/FC100; see Materials and Methods for complete descriptions).

A priori, a linear relation is expected between fluorescence and the absorption cross section of single cells (27), which implies a nonlinear relationship with the Chl *a* content given the package effect. The package effect entails that larger cells can expose relatively less pigment for light harvesting than smaller cells due to constraints imposed by the relationship between cell surface area and volume (3, 4, 28). The best fit (lowest Akaike score) between fluorescence and Chl *a* content per cell was given by a curvilinear model. We performed a linear regression over the log-log transformed data to adjust an exponential curve to the experimental data obtained with the 200×/FC50 combination ($F = 75.46 \times$ Chl $a^{0.4}$, $R^2 = 0.85$, $P < 0.001$ [where F is fluorescence and Chl *a* is the Chl a content]) (Fig. 4A) and the 100×/FC100 combination ($F = 40.63 \times$ Chl $a^{0.28}$, $R^2 = 0.91$, $P < 0.001$) (Fig. 4B).

Interspecific scaling of chlorophyll content. For each irradiance level, we combined the data for the different species and explored the relationship between Chl *a* content and cell biovolume. Figure 5 shows both the analytical Chl *a* estimates (upper panels) and the estimates derived from the FlowCam fluorescence using the fluorescence-to-Chl *a* conversions described above (lower panels), as a function of body size for the different irradiance treatments. A reduced major axis regression on the

TABLE 1 Incubation results[a]

Expt	Light (μmol photons m^{-2} s^{-1})	Day	ESD (μm)	C (pg $cell^{-1}$)	Chl *a* (pg $cell^{-1}$)	Fluorescence peak (AU/cell) (mean ± SD)[b]	μ (day^{-1})[c]	*g*
5	115	6	4.0	5.6	0.28	45 ± 20	0.29*	2.5
5	230	6	4.4	7.1	0.18	41 ± 19	0.45*	3.9
5	460	6	4.2	6.4	0.14	37 ± 18	0.57*	5.0
5	920	6	4.5	7.3	0.15	30 ± 17	0.54*	4.7
5	1,839	6	4.7	8.4	0.10	27 ± 14	0.57*	5.0
6	115	5	4.5	7.7	0.98	50 ± 22	−0.50	−2.3
6	230	5	5.1	10.6	0.86	46 ± 28	−0.45	−1.9
6	460	5	5.1	10.4	0.55	56 ± 27	−0.43	−1.3
6	920	5	5.0	10.1	0.21	55 ± 25	0.00	0.7
6	1,839	5	4.4	7.1	0.20	40 ± 21	0.37*	1.8
7	115	6	7.3	26.1	1.93	109 ± 20	0.38*	3.6
7	230	6	7.8	30.5	2.05	108 ± 20	0.66*	5.4
7	460	6	8.2	35.3	1.74	98 ± 22	0.74*	6.3
7	920	6	7.8	31.0	1.35	85 ± 23	0.91*	6.6
7	1,839	6	7.8	30.9	0.47	87 ± 25	0.35*	5.9
8	55	4	8.1	34.1	2.40	109 ± 29	0.03	0.2
8	92	4	8.6	40.1	2.23	100 ± 26	0.15	0.8
8	230	4	8.5	38.0	2.27	83 ± 25	0.23	1.3
8	382	4	9.0	44.0	2.20	100 ± 27	0.24	1.4
8	828	4	8.7	40.3	1.50	83 ± 24	0.39*	2.2
8	1,563	4	8.6	39.1	1.46	80 ± 26	0.18	1.0
8	55	6	8.4	37.4	3.42	105 ± 26	−0.06	0.0
8	92	6	8.4	36.9	3.36	105 ± 27	0.01	0.8
8	230	6	8.4	37.2	2.53	105 ± 25	0.06	1.4
8	382	6	8.6	39.8	2.03	87 ± 26	0.43*	2.7
8	828	6	8.4	36.5	1.86	88 ± 25	0.26*	2.9
8	1,563	6	9.8	55.3	1.56	99 ± 27	0.25*	1.8
9	115	6	10.1	60.5	4.42	168 ± 25	0.46*	1.1
9	230	6	10.4	65.7	3.34	154 ± 28	0.48*	2.5
9	460	6	10.3	64.9	2.48	133 ± 27	0.51*	3.3
9	920	6	10.9	73.4	1.78	115 ± 27	0.66*	3.5
9	1,839	6	10.2	62.8	1.56	106 ± 28	0.61*	3.6
10	115	6	31.2	2,018.8	30.57	101 ± 39	−0.16	−1.1
10	230	6	35.3	2,889.5	31.34	98 ± 36	−0.20	−1.1
10	460	6	33.9	2,498.7	21.64	104 ± 32	−0.18	−0.8
10	920	6	35.2	2,836.9	15.51	102 ± 29	−0.29	−1.3
10	1,839	6	37.1	3,286.7	9.89	94 ± 27	−0.19	−1.1
11	37	4	23.7	888.2	10.99	73 ± 24	−0.19	−1.1
11	69	4	23.4	867.3	7.96	76 ± 24	−0.12	−0.7
11	152	4	22.3	754.8	7.42	71 ± 26	−0.08	−0.5
11	276	4	21.4	677.8	4.55	65 ± 25	0.05	0.3
11	598	4	21.9	720.3	3.66	60 ± 26	0.07	0.4
11	1,563	4	21.5	684.3	2.53	49 ± 23	0.10	0.6
11	37	6	23.5	884.6	8.07	60 ± 24	0.04	−0.9
11	69	6	23.4	864.8	7.46	70 ± 22	−0.10	−1.0
11	152	6	22.3	756.3	6.33	72 ± 24	0.02	−0.4
11	276	6	21.2	654.6	4.94	62 ± 26	−0.06	0.1
11	598	6	21.1	642.6	3.71	55 ± 25	−0.16	−0.2
11	1,563	6	20.8	616.6	2.47	51 ± 25	−0.15	0.1
12	115	6	28.7	1,621.7	239.82	136 ± 31	−0.87	−5.6
12	230	6	30.2	1,849.0	53.34	126 ± 26	−0.20	−3.7
12	460	6	32.0	2,162.3	50.71	119 ± 29	0.04	0.4
12	920	6	32.3	2,225.8	48.86	109 ± 27	−0.19	−0.5
12	1,839	6	32.4	2,231.7	40.73	111 ± 26	−0.10	−1.7

[a]Cell size, cellular composition (carbon and analytical Chl *a*), fluorescence peak, growth rate (μ), and number of generations experienced (*g*) during the six experiments (experiments 5 to 12 [Table 1]) were gathered to estimate the conversion from fluorescence to intracellular Chl *a* and the allometry of Chl *a* content. Note that for experiments 8 and 11, the composition and growth parameters have been estimated not only for the last day of the incubation but also for the midterm sampling day (i.e., day 4).

[b]AU, arbitrary units.

[c]Asterisks indicate those cultures that kept growing in exponential phase.

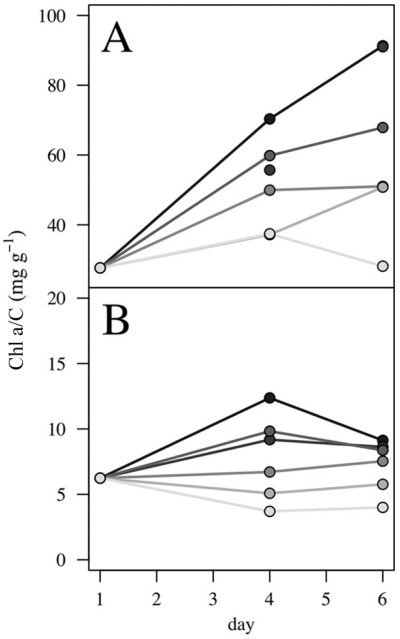

FIG 2 Relative compositions of the cells of *Rhodomonas salina* (experiment 8) (A) and *Alexandrium tamarense* (experiment 11) (B) in terms of the Chl *a*-to-carbon ratio (mg g^{-1}) as a function of incubation time in the different light treatments (graded from light to dark gray, corresponding to high to low irradiance levels).

log-transformed data was used to estimate the allometric size scaling exponent at each irradiance level (Fig. 5). The size scaling exponents were estimated additionally (dashed lines) for cultures that only kept growing in exponential phase, as indicated in Table 1. The size scaling exponents of Chl *a* content increased with irradiance from 0.65 to 0.83 (Fig. 5A to E), which translates into a decrease in the size scaling exponent with increasing light limitation (Fig. 6A). Similarly, the pattern of decrease of the size scaling exponent under light-limited conditions was captured by the FlowCam-measured fluorescence (Fig. 6B). Considering this Chl *a* content predicted from fluorescence, the

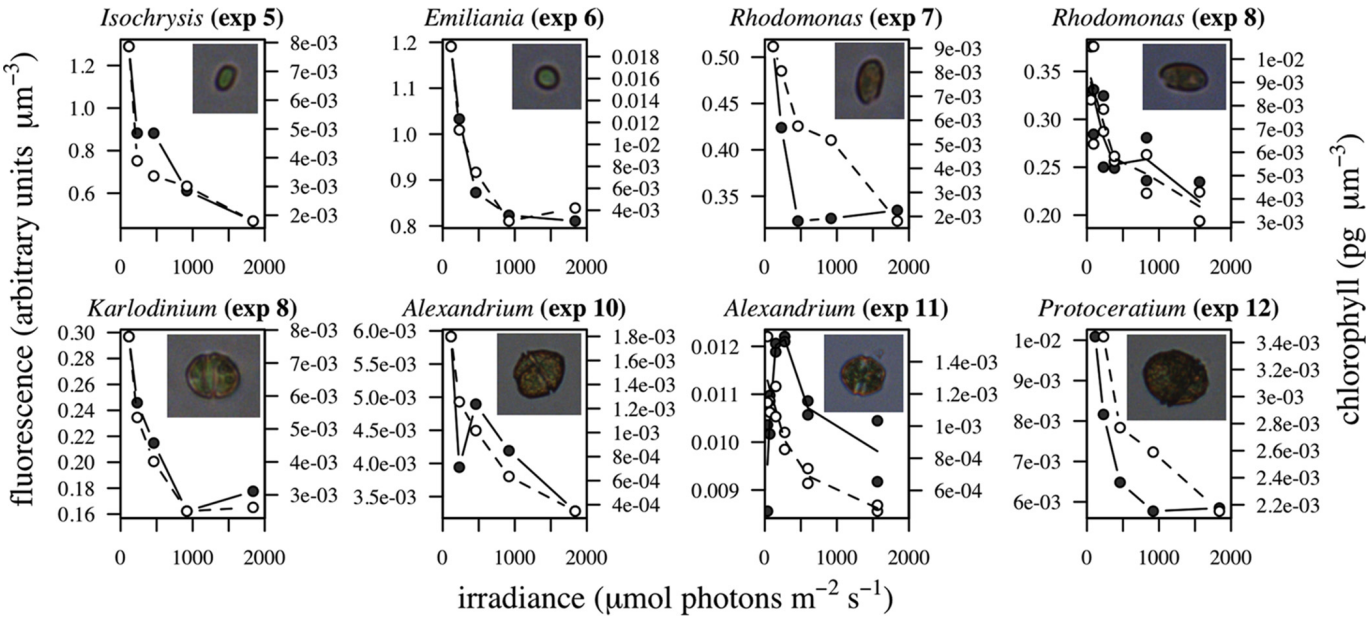

FIG 3 Incubation overview. Fluorescence per biovolume unit (black circles) and intracellular Chl *a* concentration (white circles) as a function of growth irradiance intensity (µmol photons m^{-2} s^{-1}) on the last day of each experiment.

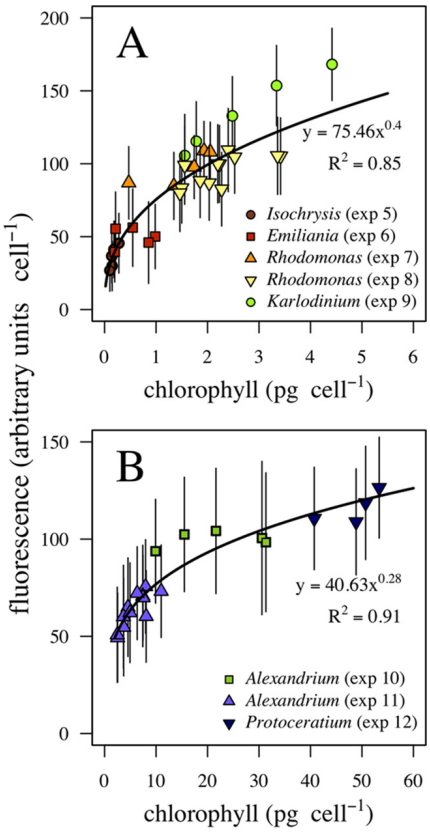

FIG 4 Fluorescence-to-Chl *a* conversion. Fluorescence peaks per cell measured by the FlowCam as a function of analytic Chl *a* per cell are shown for the experiments analyzed with the 200×/FC50 (A) and 100×/FC100 (B) lens-flow chamber combinations. Solid lines, equations, and R^2 values indicate the fitted conversion from fluorescence peak to Chl *a*.

exponents of the size dependence of pigment content at each irradiance level were slightly higher, ranging between 0.77 and 0.90 (Fig. 5F to J).

Intraspecific scaling of chlorophyll content. The measurement of fluorescence on a single-cell basis allowed us to explore the size dependence of Chl *a* content within

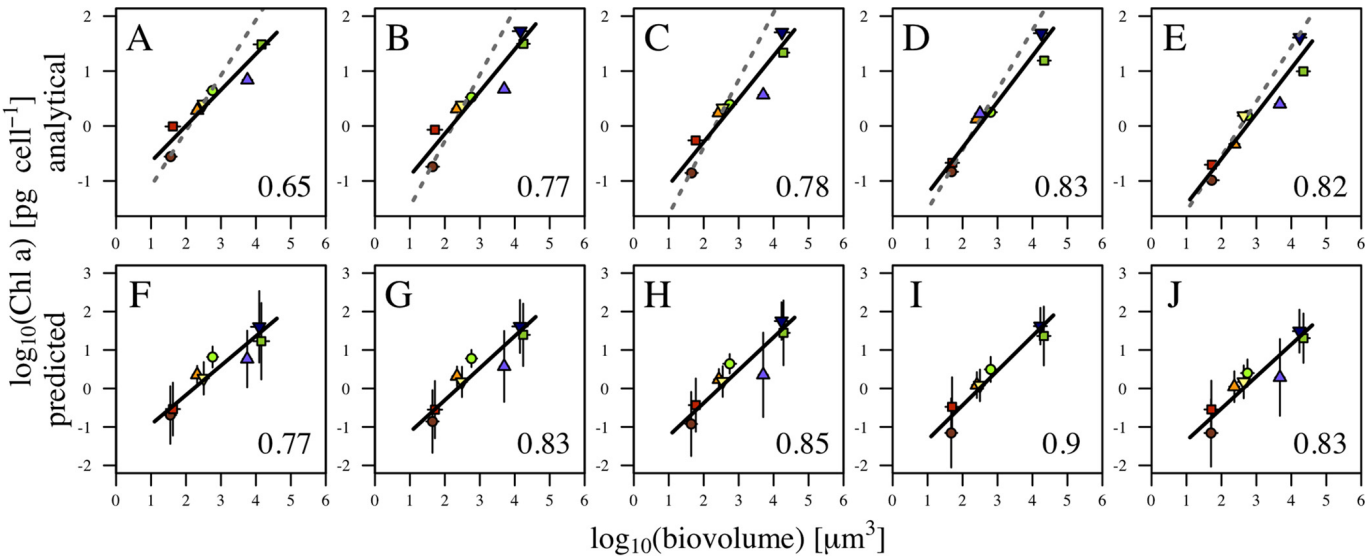

FIG 5 Interspecific size scaling of Chl *a* per cell. Results are shown of size scaling obtained by combining the results from experiments 5 to 12 for each of the increasing irradiance treatments for analytical Chl *a* (each experiment provided a unique Chl *a* value, and hence, vertical error bars are not available) (A to E) and for the increasing irradiance treatments for fluorescence-based Chl *a* (standard deviations indicated by vertical bars) (F to J). Solid lines represent results for all experiments; dashed lines in the upper panels include results for cultures only in exponential growth (Table 1).

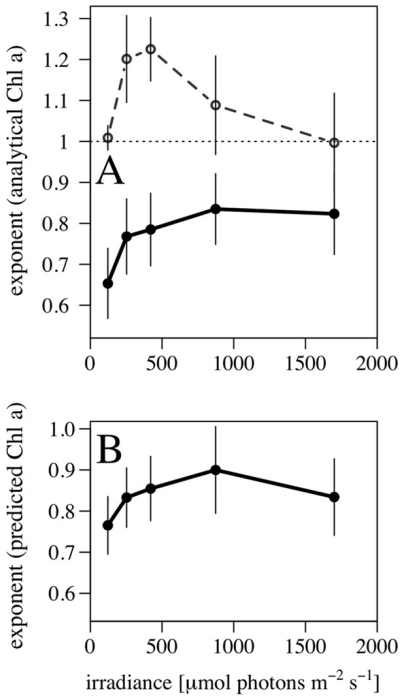

FIG 6 Size scaling exponent of Chl *a* per cell as a function of growth irradiance for analytical Chl *a* (A) and fluorescence-based Chl *a* (B). Size scaling exponents were calculated from reduced major axis regression, and standard deviations are represented by vertical bars. Solid lines represent results for all experiments, and the dashed line (upper panel) represents results only for cultures in exponential growth.

single populations. To analyze the size dependence of Chl *a* content as a function of irradiance within each treatment, the fluorescence of each single cell was converted to Chl *a* content and plotted against cellular biovolume in a log-log scale. As an example, results of the five irradiance treatments in experiment 9 (*Karlodinium veneficum* [syn., *Karlodinium micrum*]) are shown in Fig. 7 (with increasing irradiance from panels A to E). The distributions of biovolume and Chl *a* per cell were log-normal, as indicated by the bar plots in the *x* and *y* axes. The dispersion of the data and the presence of outliers are more evident at high irradiance levels. The size scaling exponent was obtained using robust linear regression, an alternative to least-squares regression that is less sensitive to outliers (29), and was tested for statistical significance.

Considering a single species, the size scaling exponent tended to decrease under light-limited conditions, similarly to what happens at the interspecific level. Figure 8 shows the variation of the size scaling exponents different from zero ($P < 0.05$) as a

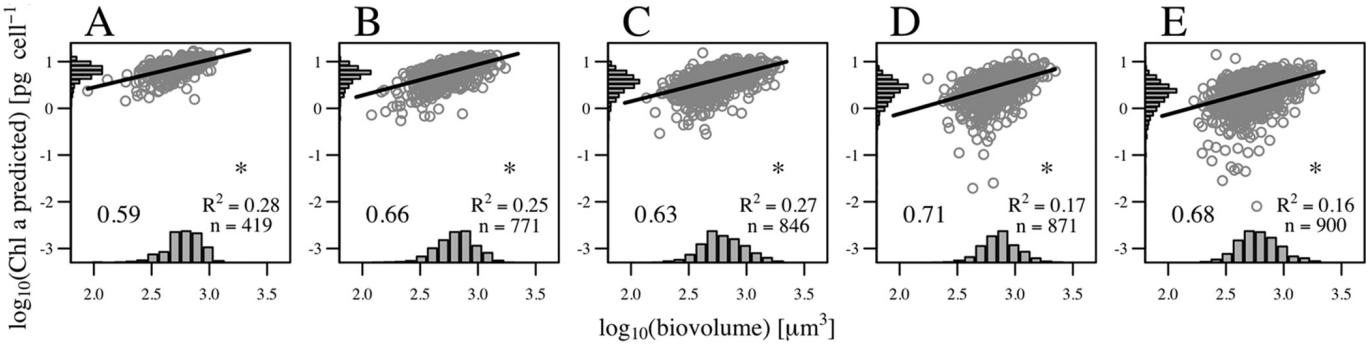

FIG 7 Intraspecific size scaling of fluorescence-based Chl *a* per cell. Population size scaling in the five increasing irradiance treatments (A to E) of experiment 9 (*K. micrum*). The size scaling exponent was obtained through robust linear regression, and the slope, R^2, of the relationship and the number of cells counted are shown in each panel. The asterisk in each panel indicates that the relationship was significant ($P < 0.05$). Bar plots attached to the *x* and *y* axes show the distribution of cell biovolume and predicted Chl *a*, respectively.

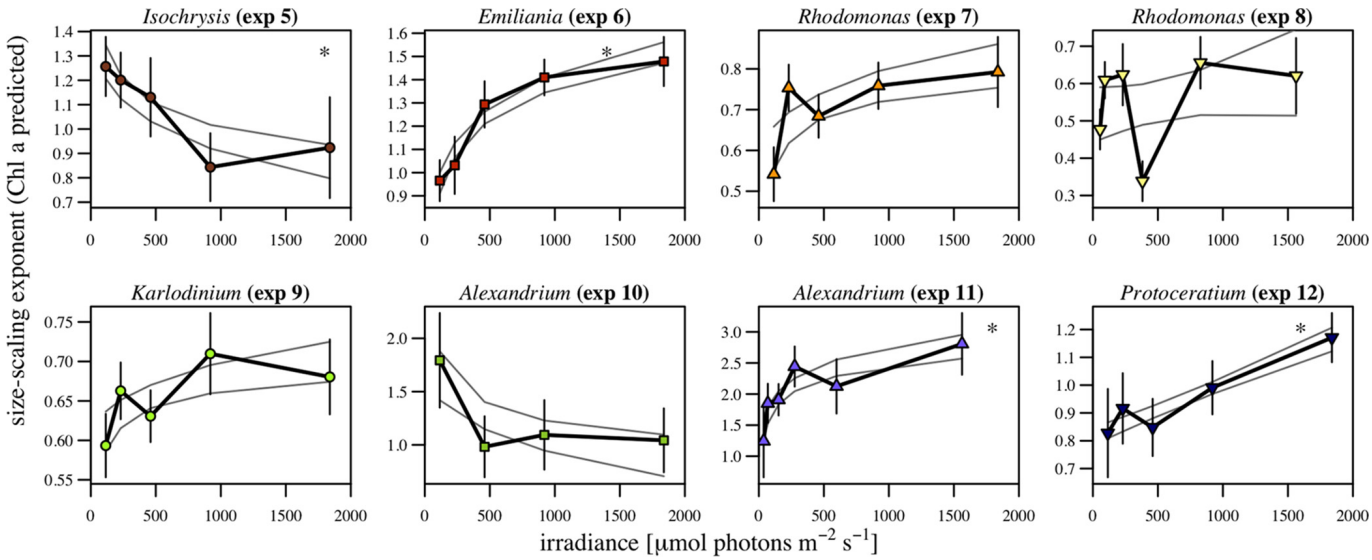

FIG 8 Change in intraspecific size scaling with light. Intraspecific size scaling exponents for fluorescence-based Chl *a* per cell as a function of growth irradiance for experiments 5 to 12 (Table 2) are shown. The size scaling exponent was calculated from robust linear regression, and standard deviations are represented by vertical bars. Solid light gray lines indicate the confidence interval of the fitting with the lowest Akaike score, and the asterisk in each panel indicates that the relationship was significant ($P < 0.05$).

function of irradiance for each of the eight experiments. To visualize the trend, we adjusted linear and logarithmic models to the data and plotted the 95% confidence interval of the model with the lowest Akaike score. All experiments except experiments 5 and 10 showed a pattern of increases in the size scaling exponent at increased growth irradiance levels. Experiment 5 did not show this pattern, probably due to the small size of *Isochrysis galbana*, which is very close to the detection limit of the FlowCam.

The intraspecific scaling exponents were not limited to 1, as found at the interspecific scale, but fluctuated between 0.35 and 3.04, with the variability within each experiment ranging between 0.1 and 1.52 units. Despite the reduced biovolume range within a single species, the relationship with body size was significant in most cases (in 41 of 42 light treatments, $P < 0.05$), and body size explained between 3 and 28% of the variability in the Chl *a* content.

Field sampling. The size scaling of Chl *a* content was reproduced in the natural samples analyzed. The fluorescence values in the two subsamples analyzed for each sample were converted to Chl *a* content and combined to estimate a size scaling exponent for each sample. The exponents of the size dependence were estimated by robust linear regression and a test for significance ($P < 0.05$). Figure 9A shows an example of the results for a natural sample, with cells imaged with the 200×/FC50 combination (light gray circles) and with the 100×/F100 combination (dark gray circles), and the linear fit. Among all samples, the size scaling exponent ranged from 0.5 to 1 (Fig. 9B), and body size explained between 27% and 59% of the variability in the predicted Chl *a* content. In natural samples, the influence of other environmental variables, such as temperature and nutrient concentrations, and the physiological (ontogenetic) status of the cells (exponential growth, stationary, or senescence phase) resulted in a poor correlation between the size scaling exponent and field irradiance.

DISCUSSION

The existence of a relationship between the fluorescence measured by flow cytometers and the Chl *a* content per cell has been described before (24), but to the best of our knowledge, this is the first time that this relationship has been explored using a FlowCam and extended to microphytoplankton. The intracellular concentration of Chl *a* has been estimated for the whole phytoplankton community and for specific compartments (30, 31), but we have shown that the simultaneous acquisition of estimates of cell size, cell abundance, and fluorescence per cell by means of a FlowCam offers an

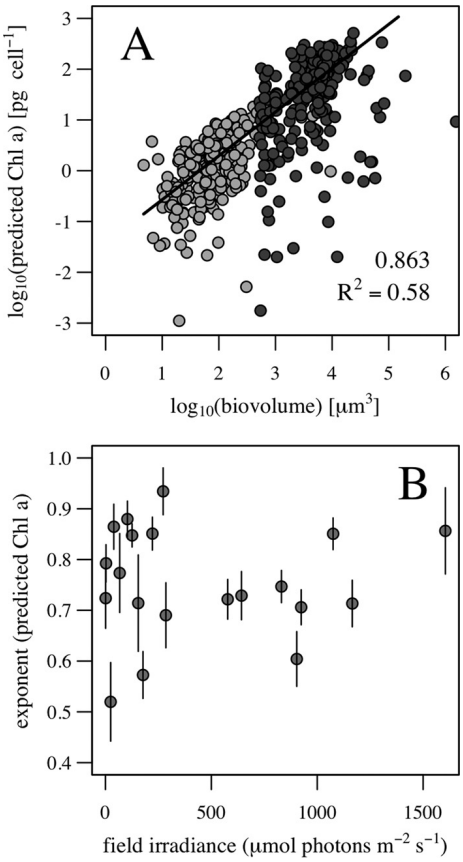

FIG 9 Application to field sampling. (A) Example of the size scaling of fluorescence-based Chl *a* per cell in a natural sample analyzed with the ×200× (light gray circles) and ×100 (dark gray circles) magnifications. The size scaling exponent was obtained through robust linear regression, and the slope and R^2 of the fitting appear within the panel. (B) Size scaling exponent of fluorescence-based Chl *a* per cell in a set of natural samples as a function of 24-h field irradiance history.

integrated methodology to estimate the intracellular concentration of Chl *a* of nano- and microphytoplankton on an individual, single-cell basis, allowing the characterization of the size dependence of Chl *a* content in natural samples.

Although useful as a proxy for Chl *a* content, there are limitations when estimating Chl *a* from fluorescence, given the presence of other energy-dissipating processes and also the variability of the fluorescence quantum yield itself. There are diverse processes competing with fluorescence to de-excite the molecule of Chl *a*, such as internal conversion, resonance energy transfer, quenching, and bleaching (32, 33), that may change the energy exchange rate, making the fluorescence signal no longer proportional to the amount of pigment. Through photochemical quenching, the liberation rate of electrons from photosystems increases due to enzymatic activity, and through nonphotochemical quenching, the heat dissipation is increased. Whereas photochemical quenching can be relevant in solar-stimulated Chl *a* fluorescence, it is negligible in laser-stimulated fluorescence, provided the flash is of high intensity and short length (34). It is not possible to inhibit heat dissipation totally, but it can be minimized if the measurements are taken on dark-adapted, nonstressed cells (35).

On the other hand, the quantum yield for chlorophyll fluorescence is not constant across species nor across physiological conditions. There are variations in the emission of fluorescence of Chl *a* under constant light conditions, which can indicate a vital cycle in Chl *a* synthesis (36). When a calibration is performed, this problem is common to all fluorometric methods for chlorophyll estimation, and reference values already account for variations in quantum yield. In our experiments, spectrofluorometry-determined Chl *a* and FlowCam-determined fluorescence suffered the same bias, and therefore we

considered the two approaches comparable. A different scenario occurs when the fluorescence measurement is applied to new samples without reference values. Since different environmental conditions, such as nutrient availability or temperature, may lead to widely different quantum yields of chlorophyll, it is a matter of debate common to all fluorometric methods that estimate chlorophyll from *in situ* fluorescence as to what extent a calibration made with a limited set of samples can be extrapolated to other samples acquired for a different range of environmental conditions.

Beyond the overall limitations, we consider that extrapolation to natural samples of the fluorescence-to-Chl *a* conversion we have obtained is reasonable because the relationship has been estimated by combining different species and different growth conditions. Previous correlations between fluorescence and Chl *a* in single cells (24) were species specific, which prevented its use on a routine basis for the estimation of Chl *a* content for the whole phytoplankton community. We found a curvilinear correlation between fluorescence and Chl *a* content that was taxon independent, and even if not independent of growth status, at least it encompassed the variability in pigment content due to growth rate.

Interspecific size dependence of chlorophyll content. A taxon-independent conversion allowed us to estimate the Chl *a* content in different cultures covering an ample size range and therefore enabling the analysis of the size scaling of chlorophyll content. Larger cells tend to have lower cellular pigment concentrations than smaller cells under similar environmental conditions (37), to counteract the package effect associated with increasing cell size (15). This means that the Chl *a* content per cell scales with size with exponents lower than 1, which is supported by geometrical considerations (3, 4). These theoretical predictions were supported by empirical data (16, 20) and are consistent with our results based on fluorescence-based Chl *a* estimates.

As growth irradiance decreased, the exponent of the size scaling of Chl *a* content decreased, as described in previous empirical works (20). All cell sizes showed incremental increases in pigment content, but relative to body size, the incremental increase in pigment was greater in smaller cells than in larger cells. Theoretical models have predicted an upper limit for an exponent of 3/4 under saturating irradiance (15), but our exponents surpassed this predicted value.

We are aware, however, that the results derived from the interspecific analyses need to be taken with caution for two reasons. The first reason is that in order to obtain cells of different sizes, it was necessary to combine different species. Changes in light-harvesting characteristics that are correlated with cell size can alter the size scaling of chlorophyll content. For example, a systematic shift in cell shape can reduce the package effect and mitigate the potential reduction in the size scaling exponent of cellular pigment concentration and growth rates (15). The second reason is that the growth status of the combined cultures must be the same, e.g., exponential. When the exponent of the size scaling of Chl *a* content was estimated only with cultures in exponential growth, the number of data were reduced and the exponents differed from those previously described (Fig. 6A). Therefore, the relevance of the size scaling exponents obtained by combining all cultures may be obscured by the fact that not all populations were in the same growth phase.

It is crucial to compare organisms with similar pigment compositions under similar growth conditions when calculating and comparing the size scaling exponents of cellular pigment concentrations. The estimation of the allometric exponents for single populations (thanks to the single-cell approach) avoids interspecific variability but also covers a size range in which all cells are in the same growth phase.

Intraspecific size dependence of chlorophyll content. At the intraspecific scale, the variability of fluorescence values, and hence Chl *a* content, was greater than that for size. Size explained only a comparatively small part of the variability of intracellular Chl *a* content because of the narrow biovolume range covered but also because of phenotypic (and to some extent also genotypic) variability among the individuals of the population and differences in the phase of the cellular cycle and physiological status.

Nevertheless, the same pattern of decrease of the size scaling exponent of Chl *a* content per cell under light-limited conditions was found when the focus was on a single species, which means that for a generalized increment in pigment content under light-limited conditions, the smaller cells had a larger margin for pigment accumulation.

This is the first time that this fact has been observed in single populations, and it means that not only do smaller species maintain higher photosynthetic rates under light limitation (38) but also that smaller cells do within the same population. The optical absorption cross section of pigments and the intracellular concentration of components that capture photon energy are physiological traits that underlie growth/production traits (39). Consequently, different cell sizes limited in the range of their plasticity for pigment content result in intraspecific differences in the integrated growth response to irradiance. Thus, the variation in the size scaling of Chl *a* content also predicts shifts in the size scaling of growth and photosynthesis with the light regime. All phytoplankton require light for growth, and the variable light regimes experienced by the cells and imposed by water column mixing may explain the size-structure of the phytoplankton community (40, 41). As a result, the differences in pigment content as a function of cell size lead to different physiological strategies and niche partitioning.

We have found that the size scaling of Chl *a* content per cell of a single population has exponents higher than 1 for some species, which means that larger cells have a higher Chl *a* content per unit volume than smaller cells. This result can be counterintuitive. It may be explained, however, if the difference in cell size and pigment content within the population is due, to great extent, to the phase of the cellular cycle experienced by the cells. In unicellular phytoplankton, within a given population, small cells are generated from larger cells, and therefore cell division may be important in reducing the package effect for young daughter cells (36). A large cell with a given Chl *a* concentration that enters the division phase of the cellular cycle will give place to two smaller cells with half the Chl *a* content, which is lower than the potential concentration that their new surface-to-volume ratio may allow. In this case, the concentration of Chl *a* will be independent of cell size, and the pigment content per cell will scale with size with an exponent of around 1. At the other extreme, a large cell can increase its pigment content above the limits imposed by its surface-to-volume ratio in order to divide this pigment between the two daughter cells, as happens with coccolithophorids (42).

For the smallest species, other biovolume constraints should be considered. Very small cells might be prevented from increasing their scalable components (photosynthetic units) due to the necessity of maintaining a constant quota of nonscalable essential components, such as the gene pool, within a very small cell biovolume (43). In this case, only those cells above a critical size will be able to increase their intracellular quota of molecules involved in metabolic processes.

Another source of uncertainty is the one related to the variability in the cellular content of other pigments. Phytoplankton cells might be able to respond to changing light levels through the production of other pigments, such as accessory light-harvesting pigments or photoprotective pigments (44). The single-cell fluorescence method accounted for the specific fluorescent signature of a given pigment, which allowed us to distinguish the patterns found for different pigments (see the supplemental material for an analysis of phycoerythrin content in *Rhodomonas salina* experiments). The pattern in size dependence of the content in a photoprotective pigment is expected to follow the opposite pattern of a light-harvesting pigment, increasing the intracellular concentration and decreasing the size scaling exponent under light-saturated conditions.

***In situ* size dependence of chlorophyll content.** Our approach, the analysis of the fluorescence signal of single cells, is a unique way to apply the same methodology to field samples and to explore the size dependence of Chl *a* content *in situ* under

different environmental conditions. It also opens the door to the estimation of size scaling per functional or taxonomic group. In this work, the natural samples yielded exponents lower than 1, in agreement with the results of interspecific size scaling. However, a question that remained unsolved is whether the upper limit of the exponent is more likely to be 1 (17) or 3/4 (15). To the best of our knowledge, we report for the first time the size scaling of Chl *a* content in single cells, and our results show maximum exponents lower than 1 but higher than 3/4, both in natural samples and in cultures. An isometric scaling between cell volume and intracellular Chl *a* has been reported on the basis of size fractionation of Chl *a* in natural samples by Marañón et al. (17), who argued that the discrepancies between the exponents obtained under natural and laboratory conditions might be due to the different growth conditions experienced by cultured cells and the small number of species used in laboratory studies.

The variability found in the intraspecific size scaling of Chl *a* content also appeared in natural samples, since different populations of the phytoplankton community present different physiologies and phases of their respective life cycles. The variation in the size scaling exponent as a function of irradiance was obscured in the field sampling, probably because the measured Chl *a* content also depends on many other factors (e.g., the nutritional status of the cells) (6). Also, we cultured only spherical or elliptical cells, but in natural communities, cells have developed strategies to escape from geometrical constraints on pigment content, as reflected in the nonspherical shapes of diatoms and the presence of vacuoles (45).

The analysis of natural samples covers a wide range of environmental scenarios, from light or nutrient limitation to saturating conditions, which can help in the understanding of how resource acquisition affects the productivity of natural communities. The size dependence of Chl *a* content relates directly to the size scaling of photosynthetic rates. This can be determinant in primary productivity models, since phytoplankton production can be modeled in a more realistic way, improving current estimates derived from global primary production models. State-of-the-art net primary production (NPP) models use carbon biomass instead of Chl *a* concentration, since variability in intracellular Chl *a* content from light acclimation and nutrient stress confounds the relationship between Chl *a* and phytoplankton biomass (46, 47). *In situ* data sets such as those obtained with the FlowCam, including cell size and Chl *a* content, can be useful in the validation of these models.

MATERIALS AND METHODS

Phytoplankton cultures and growth conditions. We performed a series of incubation experiments to induce photoacclimation in cultured phytoplankton, exposing monospecific suspensions of cells to different light intensities in order to obtain a gradient of intracellular Chl *a* concentrations. Seven species were used: *Isochrysis galbana*, *Emiliania huxleyi*, *Rhodomonas salina*, *Prorocentrum micans*, *Karlodinium veneficum* (syn., *Karlodinium micrum*), *Alexandrium tamarense*, and *Protoceratium reticulatum*. The inocula were maintained in exponential growth in F2 medium at 15°C in a culture chamber with a 12-h-light: 12-h-dark photoperiod and low light conditions. With those initial cultures, we conducted 12 experiments (Table 2).

Each experiment took place in a linear incubator illuminated at one end by a spotlight. The incubator was divided into compartments along its axis by means of transverse partitions consisting of a double layer of nylon mesh. The initial culture was divided in 50-ml CellStack culture chambers (Corning), and the chambers were placed into the compartments of the incubator. Total irradiance (photosynthetically active radiation [PAR]) in each compartment was measured with a Li-Cor radiometer (Biospherical). The irradiances varied slightly between experiments, but in any one experiment, light levels ranged between 37 and 1,838 μmol photons m^{-2} s^{-1} of PAR. By running water through the incubator, the temperature was kept stable at 15.5 $\pm$ 0.5°C. Incubations were kept with a constant photoperiod over 6 days in most cases to allow photoacclimation. Samples for analysis were taken always at 9:00 a.m., 2 h after the light was activated. The culture chambers were shaken manually twice a day.

Experiments 1 to 4 were run in duplicate, in parallel incubator lines; samples for microscopy counts, estimation of Chl *a* concentration, and *in vivo* FlowCam analysis were taken on the last day of each incubation experiment. Experiments 5 to 12 were run in a single incubator line; samples were taken on the first and last days of each incubation experiment, and additionally in the midterm of experiments 8 and 11 (Table 2).

Microscopy counts were carried out by placing 1 ml of sample in a Sedgwick-Rafter counting cell slide under a Nikon inverted microscope. For the analysis of Chl *a* concentration, 10 ml of each sample was filtered onto Whatman GF/F filters, frozen at −18°C for 24 h, and extracted in 3 ml of acetone for 24 h.

TABLE 2 Incubation conditions[a]

Expt	Species	No. of light treatments	Photoperiod (h) (light/dark)	Total no. of days	Day(s) of measurements	Lens/flow chamber	No. of points for the calibration
1	*Isochrisis galbana*	5	12/12	4	4	20×/FC50	
2	*Isochrisis galbana*	5	12/12	6	6	20×/FC50	
3	*Isochrisis galbana*	5	12/12	1	1	20×/FC50	
4	*Prorocentrum micans*	2	12/12	1	1	20×/FC50	
5	*Isochrisis galbana*	5	12/12	6	1, 6	20×/FC50	5
6	*Emiliania huxleyi*	5	12/12	5	1, 5	20×/FC50	5
7	*Rhodomonas salina*	5	12/12	6	1, 6	20×/FC50	5
8	*Rhodomonas salina*	6	14/10	6	1, 4, 6	20×/FC50	12
9	*Karlodinium micrum*	5	12/12	6	1, 6	20×/FC50	5
10	*Alexandrium tamarense*	5	12/12	6	1, 6	10×/FC100	5
11	*Alexandrium tamarense*	6	14/10	6	1, 4, 6	10×/FC100	12
12	*Protoceratium reticulatum*	5	12/12	6	1, 6	10×/FC100	5

[a]Growth conditions of the incubation experiments carried out to obtain a gradient of Chl *a* content per cell for seven different phytoplankton species are given.

Chl *a* concentration was determined using a spectrofluorometer (PerkinElmer LB-50s) with excitation set at 488 nm and emission at 663.5 nm. The signal of the spectrofluorometer was calibrated against Chl *a* solutions of known concentrations. The concentration of extracted Chl *a* was divided by the number of cells to obtain the Chl *a*-per-cell value, and the concentration of extracted Chl *a* was divided by the total cellular volume to obtain the average intracellular Chl *a* concentration.

In vivo FlowCam analysis provided measurements of cell concentration and of single-cell fluorescence and size. Excitation illumination consisted of a blue laser fan of 488 ± 0.04 nm, and fluorescence was measured as the emitted light passing a 650-nm long-pass filter reaching a photomultiplier tube (PMT 1). When the fluorescent light reaches the PMT, a voltage pulse is generated that is described numerically by three parameters: the maximum value reached by the pulse, known as height or peak, the number of consecutive measurements that exceeded the threshold value, called width, and the integrated area under the pulse. The width and the area of the pulse are indicative of particle transit time and hence are strongly influenced by the flow speed of sample analysis and the size of the cell being detected (48), while the peak of the signal is expected to reflect the total fluorescence of the cell and therefore was the parameter chosen to estimate the intracellular Chl *a* content.

Field sampling. Field data consisted of 20 samples taken from 12 to 14 April 2013 in coastal, shelf, and oceanic waters of the Cantabrian Sea (Southern Bay of Biscay) (43.51 to 43.80°N, 5.55 to 3.73°W, 25 to 1,625 m bathymetry). Seawater samples were collected at selected depths (ranging from 3 to 100 m) with Niskin bottles mounted on a rosette sampler system equipped with a CTD (conductivity-temperature-depth) probe (SBE911) and an auxiliary sensor for the measurement of underwater PAR (Biospherical/Li-Cor radiometer). Surface PAR on an hourly basis was recorded on a meteorological station sited on land near the sampling area (43.54°N, 5.62°W, at 30 m above mean sea level).

From the *in situ* PAR profile, the attenuation coefficient (k_d) was estimated with the light extinction equation

$$I_z = I_0 \times e^{(-z \times k_d)} \quad (1)$$

where I_z and I_0 represent, respectively, irradiance at a given depth and on the surface, and z is the depth in the water column. To integrate the irradiance regime experienced by the cells of a given sample, the field irradiance at the sample depth was estimated by taking into account the 24-h PAR regime prior to the time of acquisition of the sample (only light hours), calculated from surface solar radiation and assuming a constant k_d, and weighting the calculated underwater PAR by the elapsed time. Field irradiances ranged from 1 to 1,604 μmol photons m^{-2} s^{-1}.

Phytoplankton samples were analyzed onboard with the FlowCam. They were maintained fresh and in the dark until analysis, which started immediately after collection to minimize pigment degradation. Each sample was split in two: an unconcentrated subsample prefiltered at 40 μm for analysis with ×200 magnification and a 50-μm flow chamber (1 ml) (200×/FC50) and a concentrated subsample prefiltered at 100 μm (1 liter down to around 20 ml) for analysis with ×100 magnification and a 100-μm flow chamber (10 ml) (100×/FC100). The sample concentration was carried out by reverse filtration (49) through a 15-μm mesh to prevent the damage of living cells. A detailed description of the protocol for FlowCam sample analysis can be found elsewhere (50).

Data analysis. For each sample, either cultured or natural, the abundance of autotrophic cells was estimated from all cells imaged by the FlowCam in the fluorescence-triggered mode. The size of the cells was estimated by considering only properly focused and uncut single cells. The equivalent spherical diameter (ESD) and geometrical section of each cell were obtained directly from the digital image taken by the FlowCam, and particle biovolume was calculated as a revolution volume from the ESD of the particles. Fluorescence signals were selected by considering only uncut cells captured in the proximities of the laser beam. FlowCam photographs with more than one particle were rejected.

Experiments 1 to 4 were used to explore the variability in fluorescence measurements, in parallel lines of the incubator (experiments 1 to 4) and in replicate analysis of the same sample (experiment 1). Experiments 5 to 12 were used to obtain a fluorescence-to-Chl *a* conversion and to explore the inter- and intraspecific scaling of chlorophyll content. We categorized the day of sample extraction according to the

growth phase of the culture, as being in exponential phase or not, by plotting the evolution of carbon biomass. From the initial carbon content (C_0 at time t_0) to the content in the last day of sample extraction (C_t at time t), we estimated the specific growth rate (μ)

$$C_t = C_0 \times e^{\mu(t - t_0)} \quad (2)$$

and the number of generations (g) experienced by the population from the initial sample

$$g = \log_2(C_t/C_0) \quad (3)$$

To check whether the photoacclimation had been completed at the end of the incubations, we compared the carbon and chlorophyll cell contents between the midterm and the last sample day of experiments 8 and 11 (days 4 and 6, respectively).

SUPPLEMENTAL MATERIAL

Supplemental material for this article may be found at https://doi.org/10.1128/AEM.03317-16.

SUPPLEMENTAL FILE 1, PDF file, 0.32 MB.

ACKNOWLEDGMENTS

We are indebted to the Red Tides and Harmful Algae team of the Centro Oceanográfico de Vigo (IEO) for the supply of clones from their Toxic Phytoplankton Culture Collection. We thank the captain and crew of the B/O *Ángeles Alvariño* for their assistance during the RADCAN 0413 cruise. F. Ronzón kindly provided solar radiation data from his meteorological station in Gijón.

This work was supported by the Fundación para el Fomento en Asturias de la Investigación Científica Aplicada y la Tecnología (FICYT) (research grant BP07-081 to E.A.), the Ministerio de Economía y Competitividad (MINECO) (projects CTM2006-04854-MAR and CTM2009-13882-MAR to E.N. and A.L.-U.), and the Instituto Español de Oceanografía (IEO) (project RADIALES). The publication of this paper was funded by the Principado de Asturias (project GIDEP, GRUPIN14-144).

REFERENCES

1. Cullen JJ. 1982. The deep chlorophyll maximum: comparing vertical profiles of chlorophyll a. Can J Fish Aquat Sci 39:791–803. https://doi.org/10.1139/f82-108.
2. MacIntyre HL, Kana TM, Anning J, Geider RJ, Anning T, Geider RJ. 2002. Photoacclimation of photosynthesis irradiance response curves and photosynthetic pigments in microalgae and cyanobacteria. J Phycol 38:17–38. https://doi.org/10.1046/j.1529-8817.2002.00094.x.
3. Kirk JTO. 1975. A theoretical analysis of the contribution of algal cells to the attenuation of light within natural waters. II. Spherical cells. New Phytol 75:21–36. https://doi.org/10.1111/j.1469-8137.1975.tb01367.x.
4. Kirk JTO. 1975. A theoretical analysis of the contribution of algal cells to the attenuation of light within natural waters. I. General treatment of suspensions of pigmented cells. New Phytol 75:11–20.
5. Huot Y, Babin M, Bruyant F, Grob C, Twardowski MS, Claustre H. 2007. Does chlorophyll a provide the best index of phytoplankton biomass for primary productivity studies? Biogeosci Discuss 4:707–745. https://doi.org/10.5194/bgd-4-707-2007.
6. Geider RJ. 1987. Light and temperature dependence of the carbon to chlorophyll a ratio in microalgae and cyanobacteria. New Phytol 106:1–34. https://doi.org/10.1111/j.1469-8137.1987.tb04788.x.
7. Geider RJ, MacIntyre HL, Kana TM. 1998. A dynamic regulatory model of phytoplanktonic acclimation to light, nutrients, and temperature. Limnol Oceanogr 43:679–694. https://doi.org/10.4319/lo.1998.43.4.0679.
8. Tang EPY. 1996. Why do dinoflagellates have lower growth rates? J Phycol 32:80–84. https://doi.org/10.1111/j.0022-3646.1996.00080.x.
9. Riemann B, Simonsen P, Stensgaard L. 1989. The carbon and chlorophyll content of phytoplankton from various nutrient regimes. J Plankt Res 11:1037–1045. https://doi.org/10.1093/plankt/11.5.1037.
10. Cullen JJ, Yang X, MacIntyre HL. 1992. Nutrient limitation of marine photosynthesis, p 70–88. *In* Falkowski PG, Woodhead AD (ed), Primary productivity and biogeochemical cycles in the sea. Springer, New York, NY.
11. Yacobi YZ, Zohary T. 2010. Carbon:chlorophyll *a* ratio, assimilation numbers and turnover times of Lake Kinneret phytoplankton. Hydrobiologia 639:185–196. https://doi.org/10.1007/s10750-009-0023-3.
12. Geider RJ, Platt T, Raven JA. 1986. Size dependence of growth and photosynthesis in diatoms: a synthesis. Mar Ecol Prog Ser 30:93–104. https://doi.org/10.3354/meps030093.
13. Finkel ZV. 2001. Light absorption and size-scaling of light-limited metabolism in marine diatoms. Limnol Oceanogr 46:86–94. https://doi.org/10.4319/lo.2001.46.1.0086.
14. Mei ZP, Finkel ZV, Irwin AJ. 2009. Light and nutrient availability affect the size-scaling of growth in phytoplankton. J Theor Biol 259:582–588. https://doi.org/10.1016/j.jtbi.2009.04.018.
15. Finkel ZV. 2004. Resource limitation alters the 3/4 size scaling of metabolic rates in phytoplankton. Mar Ecol Prog Ser 273:269–279. https://doi.org/10.3354/meps273269.
16. Key T, McCarthy A, Campbell DA, Six C, Roy S, Finkel ZV. 2010. Cell size trade-offs govern light exploitation strategies in marine phytoplankton. Environ Microbiol 12:95–104. https://doi.org/10.1111/j.1462-2920.2009.02046.x.
17. Marañón E, Cermeño P, Rodríguez J, Zubkov MV, Harris RP. 2007. Scaling of phytoplankton photosynthesis and cell size in the ocean. Limnol Oceanogr 52:2190–2198. https://doi.org/10.4319/lo.2007.52.5.2190.
18. Pérez V, Fernández E, Marañón E, Morán XAG, Zubkov MV. 2006. Vertical distribution of phytoplankton biomass, production and growth in the Atlantic subtropical gyres. Deep Sea Res Part I Oceanogr Res Pap 53:1616–1634. https://doi.org/10.1016/j.dsr.2006.07.008.
19. Harrison PJ, Conway HL, Holmes CR, Davis CO. 1990. Effects of nutrients and light on the biochemical composition of phytoplankton. J Appl Phycol 2:45–56. https://doi.org/10.1007/BF02179768.
20. Fujiki T, Taguchi S. 2002. Variability in chlorophyll a specific absorption coefficient in marine phytoplankton as a function of cell size and irradiance. J Plankton Res 24:859–874. https://doi.org/10.1093/plankt/24.9.859.
21. Yentsch CM, Horan PK, Muirhead K, Dortch Q, Hangen F, Legendre L, Murphy LS, Perry MJ, Phinney DA, Pomponi SA, Spinrad RW, Wood M, Yentsch CS, Zahuranec BJ. 1983. Flow cytometry and cell sorting: a technique for analysis and sorting of aquatic particles. Limnol Oceanogr 28:1275–1280. https://doi.org/10.4319/lo.1983.28.6.1275.

22. Lorenzen CJ. 1966. A method for the continuous measurement of in vivo chlorophyll concentration. Deep Sea Res 13:223–227.
23. Yentsch CS, Menzel DW. 1963. A method for the determination of phytoplankton chlorophyll and phaeophytin by fluorescence. Deep Sea Res 10:221–231.
24. Sosik HM, Chisholm SW, Olson RJ. 1989. Chlorophyll fluorescence from single cells: interpretation of flow cytometric signals. Limnol Oceanogr 34:1749–1761. https://doi.org/10.4319/lo.1989.34.8.1749.
25. Sieracki CK, Sieracki ME, Yentsch CS. 1998. An imaging-in-flow system for automated analysis of marine microplankton. Mar Ecol Prog Ser 168: 285–296. https://doi.org/10.3354/meps168285.
26. Steinberg MK, First MR, Lemieux EJ, Drake LA, Nelson BN, Kulis DM, Anderson DM, Welschmeyer NA, Herring PR. 2012. Comparison of techniques used to count single-celled viable phytoplankton. J Appl Phycol 24:751–758. https://doi.org/10.1007/s10811-011-9694-z.
27. Perry MJ, Porter SM. 1989. Determination of the cross-section absorption coefficient of individual phytoplankton cells by analytical flow cytometry. Limnol Oceanogr 34:1727–1738. https://doi.org/10.4319/lo.1989.34.8.1727.
28. Morel A, Bricaud A. 1986. Inherent optical properties of algal cells including phytoplankton: theoretical and experimental results. *In* Platt T, Li WKW (ed), Photosynthetic picoplankton. Can Bull Fish Aquat Sci 214:521–559.
29. Venables WN, Ripley BD. 2002. Modern applied statistics with S, 4th ed. Springer, New York, NY.
30. Sathyendranath S, Stuart V, Nair A, Oka K, Nakane T, Bouman H, Forget M-H, Maass H, Platt T. 2009. Carbon-to-chlorophyll ratio and growth rate of phytoplankton in the sea. Mar Ecol Prog Ser 383:73–84. https://doi.org/10.3354/meps07998.
31. Wang XJ, Behrenfeld MJ, Le Borgne R, Murtugudde R, Boss E. 2009. Regulation of phytoplankton carbon to chlorophyll ratio by light, nutrients and temperature in the equatorial Pacific Ocean: a basin-scale model. Biogeosci Discuss 5:3869–3903.
32. Falkowski PG, Kiefer DA. 1985. Chlorophyll a fluorescence in phytopankton: relationship to photosynthesis and biomass. J Plankton Res 7:715–731. https://doi.org/10.1093/plankt/7.5.715.
33. Sakshaug E, Bricaud A, Dandonneau Y, Falkowski PG, Kiefer DA, Legendre L, Morel A, Parslow J, Takahashi M. 1998. Parameters of photosynthesis: definitions, theory and interpretation of results. J Plankton Res 19:1637–1670.
34. Bradbury M, Baker NR. 1981. Analysis of the slow phases of the in vivo chlorophyll fluorescence induction curve. Changes in the redox state of photosystem II electron acceptors and fluorescence emission from photosystems I and II. Biochim Biophys Acta 635:542–551.
35. Maxwell K, Johnson GN. 2000. Chlorophyll fluorescence—a practical guide. J Exp Bot 51:659–668. https://doi.org/10.1093/jexbot/51.345.659.
36. Baird ME, Ralph PJ, Rizwi F, Wild-Allen K, Steven ADL. 2013. A dynamic model of the cellular carbon to chlorophyll ratio applied to a batch culture and a continental shelf ecosystem. Limnol Oceanogr 58: 1215–1226. https://doi.org/10.4319/lo.2013.58.4.1215.
37. Agustí S. 1991. Allometric scaling of light absorption and scattering by phytoplankton cells. Can J Fish Aquat Sci 48:763–767. https://doi.org/10.1139/f91-091.
38. Dubinsky Z, Stambler N. 2009. Photoacclimation processes in phytoplankton: mechanisms, consequences, and applications. Aquat Microb Ecol 56:163–176. https://doi.org/10.3354/ame01345.
39. Edwards KF, Thomas MK, Klausmeier CA, Litchman E. 2015. Light and growth in marine phytoplankton: allometric, taxonomic, and environmental variation. Limnol Oceanogr 60:540–552. https://doi.org/10.1002/lno.10033.
40. Karentz D, Cleaver JE, Mitchell DL. 1991. Cell survival characteristics and molecular responses of Antarctic phytoplankton to ultraviolet-B radiation. J Phycol 27:326–341. https://doi.org/10.1111/j.0022-3646.1991.00326.x.
41. Finkel ZV, Vaillancourt CJ, Irwin AJ, Reavie ED, Smol JP. 2009. Environmental control of diatom community size structure varies across aquatic ecosystems. Proc Biol Sci 276:1627–1634. https://doi.org/10.1098/rspb.2008.1610.
42. Klaveness D. 1972. Coccolithus huxleyi (Lohm.) Kamptn II. The flagellate cell, aberrant cell types, vegetative propagation and life cycles. Br Phycol J 7:309–318.
43. Raven JA. 1998. Small is beautiful: the picophytoplankton. Funct Ecol 12:503–513. https://doi.org/10.1046/j.1365-2435.1998.00233.x.
44. Lutz VA, Sathyendaranath S, Head EJH, Li WKW. 2001. Changes in the in vivo absorption and fluorescence excitation spectra with growth irradiance in three species of phytoplankton. J Plankton Res 23:555–569. https://doi.org/10.1093/plankt/23.6.555.
45. Raven JA, Callow JA. 1997. The vacuole: a cost-benefit analysis, p 59–82. *In* Leigh RA, Sanders D (ed), The plant vacuole. Academic Press, San Diego, CA.
46. Behrenfeld MJ, Boss E, Siegel DA, Shea DM. 2005. Carbon-based ocean productivity and phytoplankton physiology from space. Global Biogeochem Cycles 19:GB1006.
47. Westberry T, Behrenfeld MJ, Siegel DA, Boss E. 2008. Carbon-based primary productivity modeling with vertically resolved photoacclimation. Global Biogeochem Cycles 22:GB2024.
48. Shapiro HM. 1941. Practical flow cytometry, 4th ed. Wiley-Liss, Hoboken, NJ.
49. Dodson AN, Thomas WH. 1978. Reverse filtration, p 104–107. *In* Sournia A (ed), Phytoplankton manual. UNESCO, Paris, France.
50. Álvarez E, Moyano M, López-Urrutia Á, Nogueira E, Scharek R. 2014. Routine determination of plankton community composition and size structure: a comparison between FlowCAM and light microscopy. J Plankton Res 36:170–184. https://doi.org/10.1093/plankt/fbt069.